J. Astrophys. Astr. (1981) **2,** 215–244

Mass Segregation in Globular Clusters

K. K. Scaria and M. K. V. Bappu *Indian Institute of Astrophysics, Bangalore 560034*

Received 1980 December 3; accepted 1981 August 27

Abstract. Photoelectric aperture-photometry of ω Cen in *U, B, V*, *R* and *I* bands has established that the cluster is bluer between 2 arcmin and 4 arcmin from the centre, than it is elsewhere. The difference in $B - I$ colour between the centre and this blue zone is $\simeq 0{\cdot}45$ mag. The core radius is found to be dependant on the wavelength band chosen for observation, the smallest core radius being for the *I* band. Equidensitometry of ω Cen in *B, V* and infrared bands shows a wavelength dependence with the cluster being nearly spherical in the infrared band. It shows a maximum ellipticity around 3 arcmin from the cluster centre. The blue contribution in this zone comes from both a diffuse background of unresolved stars and an increase in the relative abundance of horizontal branch (HB) stars. The similarity between the diffuse background and the HB stars has been demonstrated. A photographic subtraction technique is used to study the distribution of HB stars in the cluster.

Results of equidensitometry of the cluster 47 Tuc, obtained in the present study, are compared with the earlier results of photoelectric photometry. Here too an increase in ellipticity is associated with an increase in the blueness of the cluster. All globular clusters studied so far for ellipticity show a similarity in the dependence of the ellipticity on the distance from the centre. The ellipticity has small values near the centre and in the outer regions, with the maximum value in between. We suggest that the red stars in globular clusters have a nearly spherical distribution. The blue stars form a bulge around the core with a more elliptical distribution and a different orientation. A similarity between the ellipticity aspects of both the globular clusters and rotation in the nucleus of M 31 is pointed out; the M 31 nucleus may thus show a bluer colour and smaller UV excess around the region where the rotation curve shows a peak.

Key words: globular clusters—ω Centauri—photoelectric photometry of globular clusters—equidensitometry—horizontal branch stars

1. Introduction

Relaxation times in globular clusters are short compared to their ages and hence these objects must be in a state of dynamical equilibrium. Hence the equipartition of energy in these clusters will cause a stratification of stars; the large mass stars would be concentrated towards the centre and the low mass stars predominate the outer regions. In an old stellar system, stars of larger mass are the red stars and a concentration of these stars towards the centre will make the system look redder at the centre. Evidence of this kind is available. Gascoigne and Burr (1956) have shown that 47 Tuc is redder at the centre by $P - V = 0{\cdot}17$ mag. Chun and Freeman (1979) find that 47 Tuc becomes bluer beyond 2 arcmin from the centre. They have made concentric aperture observations of 24 globular clusters and find that 8 of them show an increase in reddening towards the centre. King (1962) has pointed out the importance of relaxation, in very old stellar systems following mass loss, due to stellar evolution. Martin (1938) observed the RR Lyr stars in ω Cen to be less concentrated towards the centre of the cluster. The clusters M 3, M 5 and M 15 also show similar characteristics in the distribution of RR Lyr stars. Oort and van Herk (1959) have tried to explain this feature on the basis of mass loss during the evolution from the tip of the giant branch to the horizontal branch. The loss of mass at these phases of evolution gives these stars a higher velocity dispersion and hence a larger spatial distribution. An alternative interpretation can be that a radial colour gradient may indicate an abundance gradient, since the morphology of the horizontal branch is sensitive to abundance.

In a rotating cluster the segregation effect may cause different degrees of flattening for the groups of large mass and low mass stars. Many of the globular clusters are found to be elliptical in form. Dickens and Woolley (1967) have shown that the flattening of ω Cen can be explained by its rotation. The segregation effects are best seen in the inner regions of the cluster, since stellar encounters are more frequent in this region. It is impossible to study such segregation effects near the centre in a globular cluster, because of the large density of stars. But it is possible that these effects may produce changes in colour depending on the location in the cluster. We have used the photoelectric and the photographic techniques to study the colour changes indicative of these effects over the cluster ω Cen and also over 47 Tuc.

2. Photoelectric photometry of ω Centauri

The bulk of photoelectric measurements available in the literature for globular clusters are in the *U, B* and *V* bands. For old stellar systems like globular clusters, there is a predominance of light in the longer wavelengths and hence the *R* and *I* bands would be valuable sources of information. We have therefore employed the five colour *UBVRI* photometry for this study.

The cluster ω Cen is a very good candidate for a study of the colour gradient, because it is the most massive cluster in our galaxy. It has the largest core radius among the brightest galactic globular clusters. There is no evidence of non-uniform reddening over the cluster, even though it is only 15° above the galactic plane. Star counts of Lindsay (1956) and the observations on the horizontal and the giant branches of the cluster by Freeman and Rodgers (1975) and Norris and Bessell (1975)

show that there is no large scale differential interstellar reddening across the cluster. We also find from the equidensitometry of photographs obtained in different wavelength bands, that there is no asymmetric absorption over the cluster. The major axis of the cluster is inclined by 10° to the east-west direction. There is also some evidence to the fact that the axis of rotation is perpendicular to the line of sight (Poveda and Allen 1975). Hence, we take the east-west scan as representative of the intensity gradient along the major axis and the north-south scan as indicative of the gradient along the minor axis. The relaxation time of the cluster is quite long; but since the cluster age is greater than one relaxation time (Peterson and King 1975), it has had enough time to reach a state of dynamical equilibrium.

2.1 *The Observations*

Spot measurements of brightness over the cluster were made on four consecutive nights in the month of May 1979. On each night one scan was obtained along both the east-west and north-south directions. The photometry on the cluster was done with the 102-cm reflector at Kavalur. A dry-ice cooled EMI 9558 B tube was used as the detector at the (*f*/13) Ritchey-Chrétien focus. This was followed by a pulse counting equipment and an on-line computer. Since ω Cen has an appreciable ellipticity, concentric aperture measures are not likely to yield a correct gradient of brightness in the cluster. Hence, the aperture photometry was planned along two directions in the cluster. The aperture used for the spot measurements has a diameter of 40 arcsec. The star-changing device on the telescope is a programmable facility that moves the telescope in a and δ by known amounts from a reference point, with an accuracy of 1 arcsec. The backlash in the system is less than 1 arcsec. Thus the aperture can be positioned quite accurately over the cluster, with reference to a star in the field. The star P in Fig. 14 is used as the reference star for scanning the cluster in the east-west direction while the star Q functioned as the reference star for north-south direction. The counts had a high degree of stability; the values were consistent on all the nights for each scan location. The nights used for observations were of high photometric quality. Due to the large declination, the cluster was observed every day for only about two hours around the time of culmination. The filter combination is similar to that used by Fernie (1974) except for the fact that in the *R* combination, RG 8 was used in place of RG 6. The *UBVRI* filter system was calibrated using 20 standard stars from the list of Iriarte *et al.* (1965). The comparison stars used in the cluster are marked B and D in Fig. 14. They have also been used as standard stars earlier by Arp (1958), Geyer (1967) and Dickens and Woolley (1967). Extinction coefficients and transformation coefficients for conversion to the standard Johnson *UBVRI* system, were derived for each night. Sky corrections become more and more important as we go to the outer regions of the cluster. Hence much care has been taken to make accurate measurements of the sky brightness. A relatively star-free region near the standard star D was chosen from a well exposed plate of ω Cen; the telescope was moved to this starfree region to get the sky brightness in *U, B, V, R* and *I* bands before and after a set of 3 to 4 measurements over the cluster. The sky correction applied in each band is the mean of the values obtained before and after the measurements over the cluster.

The cluster centre has been determined by the equidensitometric technique with reference to the stars T and M. The photoelectric scan paths are 10 arcsec to the west and 5 arcsec to the south of the centre thus defined. Since the diaphragm used for the scans is 40 arcsec in size, we do not consider the error, in the location of origin, to cause any inaccuracy.

2.2 *Evaluation of Errors in Photometry*

The problem of errors involved in surface photometry of globular clusters is explained in detail by King (1966b), Illingworth and Illingworth (1976), Da Costa (1979) and Chun and Freeman (1979). These authors show that the sampling and the centering errors are the most important errors encountered in surface photometry. In the case of bright globular clusters like ω Cen, the principal contribution is likely to be from sampling errors and hence we consider these in detail.

An unavoidable source of error in surface photometry of globular clusters arises from the statistical fluctuations in the number of stars of a given luminosity contained in the finite sample selected by the aperture (King 1966b). The mean relative error (σ/L) is proportional to $L^{-1/2}$ where L is the total luminosity given by $L = \Sigma\, L_i\, N_i$. Illingworth and Illingworth give the formula for the sampling errors in $\log f_V$, where f_V is the surface brightness in the V band, as

$$E_{sa} = 0{\cdot}4343\ (\sigma/L)_V \left[\frac{\text{dex } 0{\cdot}4\ (10 - m_{er})}{L_{obs}}\right]^{1/2}. \tag{1}$$

Here $(\sigma/L)_V$ is the sampling error for the model corresponding to the total integrated magnitude M_V, $m_{er} = (m - M)_{app,V} + M_V$ *and* L_{obs} is the total brightness in the aperture used for the scan expressed in units of $V = 10{\cdot}0$ mag.

Illingworth and Illingworth (1976) give a value of 0·023 for $(\sigma/L)_V$ *at* $M_V = -8{\cdot}5$ and 0·020 for $(\sigma/L)_B$ at $M_B = -7{\cdot}8$ based on the M 3 model of Sandage (1957).

When sampling errors are calculated in magnitudes, these values are to be multiplied by 2·5. If the surface brightness profile is folded at the centre to give a mean surface brightness over the cluster, then the errors obtained as above should be divided by $\sqrt{2}$.

Sampling errors in colour are calculated from Sandage's (1957) luminosity function of M 3 by Chun and Freeman (1979) using the equation

$$\sigma_c^2 = (1{\cdot}085)^2 \sum N_i \left[\frac{L_{vi}}{L_v} - \frac{L_{bi}}{L_b}\right]^2 \tag{2}$$

where L_{vi} is the visual luminosity of the stars of class i, and L_v the total visual luminosity *etc.* Chun and Freeman give values of 0·46 $(\sigma/L)_B$ and 0·51$(\sigma/L)_B$ for σ_{U-B} and σ_{B-V} respectively. The sampling error in the magntiude units is calculated as

$$E_c = 1{\cdot}086 \times 10^{-2}\, \sigma_c\ (L_{obs})^{-1/2} \tag{3}$$

where L_{obs} is the total blue brightness in the aperture expressed in the units of $B = 10{\cdot}0$ mag.

Since our photometry is in the U, B, V, R and I bands, we need the estimates of sampling errors for the R and I bands also. Instead of taking the luminosity function of a fairly metal rich cluster like M 3, we have chosen the luminosity function of the metal poor cluster M 92. This cluster compares well with ω Cen in both the metal abundance and the geometrical form. The V luminosity function for M 92 has been published by Hartwick (1970). Sandage (1970) has published the *UBV* photometry of stars in M 92 in the range from $V = 16{\cdot}26$ to $V = 22{\cdot}26$. Cathey (1974) has published the *UBVR* observations from $V = 12{\cdot}19$ to $V = 15{\cdot}41$ and Rusev (1974) has listed *BVI* magnitudes in the range $V = 12{\cdot}16$ to $V = 14{\cdot}19$. Using the above data, we have estimated the sampling errors as explained in the following.

Hartwick's (1970) luminosity function has a step size of 0·1 mag between $V = 11{\cdot}9$ to $V = 21{\cdot}1$. We have calculated the sampling errors in V directly by using the equation

$$\sigma/L = \sum_i (L_i^2\, N_i)^{1/2} \Big/ \sum_i (L_i\, N_i). \tag{4}$$

In order to estimate the sampling errors in the rest of the bands, we have treated each step in the V magnitudes as a box consisting of identical stars with constant colours. For each of these boxes, we estimate the mean colours $U - V$, $B - V$, $V - R$ and $V - I$ using the photometric data cited above. Due to the limitation in the published photometry, we could obtain the colours $V - R$ only for $V \leqslant 15{\cdot}5$ and $V - I$ only for $V \leqslant 14{\cdot}5$ while $U - V$ and $B - V$ colours are available for the entire range of $V \leqslant 21{\cdot}1$. These colours are used in estimating the luminosity in U, B, V, R and I bands for stars in each box with a given V magnitude to the limits of the available photometry. The sampling errors are then derived using equation (4) to these limits. The errors in colours are also derived similarly using equation (2). The limits of available photometry, which have forced us to truncate the luminosity function in each band or colour are enumerated below.

Case A: U, B, V band and $U - B$, $B - V$ colours for the full range of $V \leqslant 21{\cdot}1$
Case B: R band and $V - R$ colour for stars with $V \leqslant 15{\cdot}5$
Case C: I band and $R - I$ colour for stars with $\leqslant 14{\cdot}5$

In order to estimate the sampling error in R, I, $V - R$ and $R - I$ for the full range $\leqslant 21{\cdot}1$), we have studied the effect of truncating the luminosity function at $V \leqslant 15{\cdot}5$ and $V \leqslant 14{\cdot}5$ in the case of U, B, V, $U - B$ and $B - V$. Table 1(a) lists the value of (σ/L) for these three cases while Table 1(b) lists the values of $\sigma/(\sigma/L)_B$. The ratios of Case A and Case B, and of Case A and Case C are shown in the last two columns. The values for U, B, V, $U - B$ and $B - V$ are computed directly in all the three cases. The values corresponding to R and $V - R$ are computed directly only for the Cases B and C. The values for I and $R - I$ are computed only for Case C. A comparison of (σ/L) in U, B and V shows that the ratios A/B and A/C gradually increase towards longer wavelengths. This is due to the relative increase in the contribution of the brighter stars to the total luminosity, without a

comparable increase in σ. One can infer thereby that the relative contribution of fainter stars to the total (σ/L) increases with wavelength· However, the rate of increase in A/B and A/C slows down as one moves to longer wavelengths. We assume an estimated value of A/B = 0·58 and A/C = 0·43 for the bands *R* and *I*. These are shown in parentheses in Table 1. The resultant estimates of the total (σ/L) in *R* and *I* bands are also shown in parentheses.

The corresponding ratios A/B and A/C do not vary appreciably between $U - B$ and $B - V$ colours. Hence we assume the values of A/B = 1·3 and A/C = 1·7 for the colours $V - R$ and $R - I$. These values as well as the estimates of errors in $V - R$ and $R - I$ appear in parentheses in coloumns 5 and 6 in Table 1.

The values of σ/L and $\sigma_c/(\sigma/L)_B$ computed by us may be compared with the values derived by previous investigators for M 3. Illingworth and Illingworth (1976) derive a value of $(\sigma/L)_V$ = 0·023 for an integrated absolute magnitude M_V = — 8·5. The apparent magnitude of our model, integrated over all the stars considered in the evaluation of (σ/L) is equal to 8·17 mag. With a distance modulus of 14·50, this gives the model an absolute magnitude M_V = — 6·33. Our value for $(\sigma/L)_V$ at this magnitude is 0·071. Similarly the absolute magnitude in the *B* band is M_B = —5·7 and the corresponding $(\sigma/L)_B$ 0·053. When sampling errors are calculated using the above constants, we get errors which are 13 per cent larger in the *V* band and 1 per cent larger in the *B* band, as compared to the errors calculated using the M 3 luminosity function. These differences are indicative of errors introduced by using different luminosity functions. Table 2 gives sampling errors calculated on the basis of both the M 3 and M 92 models. For $V - R$ and $R - I$ colours, only our estimates of errors from the M 92 model above are given.

2.3 *Results of the Photometry*

We list separately in Table 2 the results of the aperture scans for the east-west and north-south directions. Column 1 gives *r*, the distance of the aperture from the cluster centre in minutes of arc. The letter E or W with the numbers indicates

Table 1. (a) (σ/L).

Band	Case A $V \leq 21{\cdot}1$	Case B $V \leq 15{\cdot}5$	Case C $V \leq 14{\cdot}5$	A/B	A/C
U	0.035	0.087	0.140	0.402	0.250
B	0.053	0.103	0.155	0.514	0.342
V	0.071	0.126	0.176	0.563	0.403
R	(0.084)	0.143	0.195	(0.580)	(0.430)
I	(0.090)	(0.155)	0·209	(0.580)	(0.430)

(b) $\sigma_c/(\sigma/L)_B$.

Colour	Case A $V \leq 21.1$	Case B $V \leq 15.5$	Case C $V \leq 14{\cdot}5$	A/B	A/C
$U - B$	0·49	0·39	0·31	1.3	1.6
$B - V$	0·48	0·38	0·28	1·3	1·7
$V - R$	(0·35)	0·26	0·20	(1·3)	(1·7)
$R - I$	(0·50)	(0·38)	0·29	(1·3)	(1·7)
$B - I$	(0·50)	(0·38)	0·29	(1·3)	(1·7)

whether the location is to the east or west of the centre of the cluster for the major axis scan. Similarly the letters N or S for the scan along the minor axis denote the locations to the north or south of the centre. Columns 2, 5, 8, 10, 12 and 15 give the $U - B$, $B - V$, $V - R$ and $R - I$ colours and the V and B magnitudes respectively. In columns 3, 6, 13 and 16, the sampling errors are listed for $U - B$, $B - V$ colours and V, B bands calculated from the $(\sigma/L)_V$, $(\sigma/L)_B$, σ_{U-B} and σ_{B-V} values derived

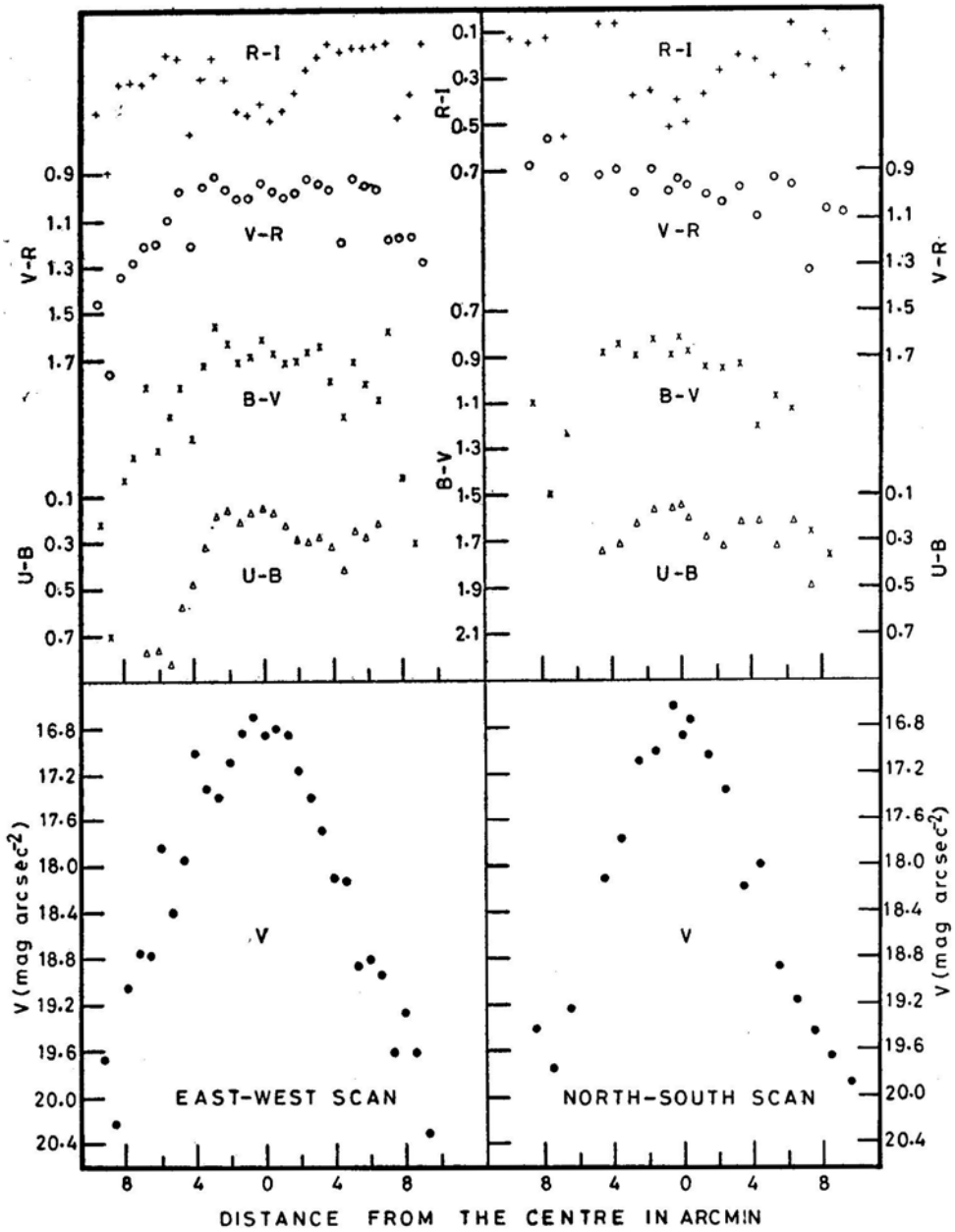

Figure 1. Results of spot measurements over the cluster ω Centauri. $U - B$, $B - V$, $V - R$ and $R - I$ colours and V magnitudes obtained for the east-west scan and the north-south scan are plotted separately.

Table 2. Values of surface brightness and colours at different locations over the cluster.

r	$U-B$	σ_{U-B} (M 3)	σ_{U-B} (M 92)	$B-V$	σ_{B-V} (M 3)	σ_{B-V} (M 92)	$V-R$	σ_{V-R} (M 92)	$R-I$	σ_{R-I} (M 92)	V	σ_V (M 3)	σ_V (M 92)	B	σ_B (M 3)	σ_B (M 92)
1	2	3	4	5	6	7	8	9	10	11	12	13	14	15	16	17
							East-West scan									
9·33W				1·62	0·31	0·29	1·46	0·21	0·44	0·30	19·67	0·46	0·52	21·29	0·61	0·61
8·67W				2·11	0·51	0·48	1·76	0·35	0·70	0·50	20·23	0·59	0·67	22·34	0·99	1·00
8·00W	1·60	0·19	0·21	1·43	0·21	0·20	1·34	0·15	0·32	0·21	19·06	0·35	0·39	20·49	0·42	0·42
7·33W	0·77	0·16	0·17	1·33	0·18	0·17	1·28	0·12	0·31	0·18	18·76	0·30	0·34	20·09	0·35	0.35
6·67W	0·76	0·14	0·15	1·02	0·16	0·15	1·21	0·11	0·32	0·16	18·78	0·30	0·34	19·80	0·31	0.31
6·00W	0·83	0·11	0·11	1·30	0·12	0·11	1·20	0·08	0·28	0·12	17·84	0·20	0·22	19·14	0·23	0·23
5·33W	0·58	0·12	0·13	1·15	0·14	0·13	1·10	0·09	0·20	0·14	18·41	0·26	0·29	19·56	0·27	0·27
4·67W	0·37	0·10	0·10	1·02	0·11	0·10	0·98	0·07	0·21	0·11	17·95	0·21	0·24	18·97	0·21	0·21
4·00W	0·48	0·07	0·07	1·25	0·08	0·07	1·21	0·05	0·53	0·08	17·02	0·14	0·15	18·27	0·15	0·15
3·33W	0·32	0·07	0·07	0·93	0·08	0·07	0·96	0·05	0·30	0·08	17·32	0·16	0·18	18·25	0·15	0·15
2·67W	0·18	0·06	0·07	0·76	0·07	0·07	0·92	0·05	0·21	0·07	17·40	0·16	0·18	18·16	0·14	0·14
2·00W	0·16	0·06	0·06	0·84	0·07	0·06	0·97	0·05	0·30	0·07	17·10	0·14	0·16	17·94	0·13	0·13
1·33W	0·21	0·06	0·06	0·91	0·06	0·06	1·01	0·04	0·44	0·06	16·85	0·13	0·14	17·76	0·12	0·12
0·67W	0·17	0·05	0·05	0·89	0·06	0·05	1·01	0·04	0·50	0·06	16·71	0·12	0·13	17·60	0·11	0·11
0·00	0·15	0·06	0·06	0·82	0·06	0·06	0·94	0·04	0·40	0·06	16·87	0·13	0·14	17.69	0·12	0.12
0·67E	0·17	0·06	0·06	0·88	0·06	0·06	0.98	0·04	0·48	0·06	16·81	0·13	0·14	17·69	0·12	0·12
1·33E	0·23	0·06	0·06	0·92	0·06	0·06	1·01	0·04	0·44	0·06	16·87	0·13	0·14	17·79	0·12	0·12
2·00E	0·29	0·06	0·06	0·91	0·07	0·07	0·99	0·05	0·36	0·07	17·18	0·15	0·17	18·09	0·14	0·14
2·67E	0·30	0·07	0·07	0·88	0·08	0·07	0·93	0·05	0·26	0·08	17·41	0·16	0·18	18·29	0·15	0·15
3·33E	0·28	0·08	0·08	0·85	0·09	0·08	0·95	0·06	0·21	0·09	17·70	0·19	0·21	18·55	0·17	0·17
4·00E	0·32	0·10	0·11	1·00	0·11	0·11	0·98	0·08	0·15	0·11	18·11	0·22	0·25	19·11	0.22	0·22
4·67E	0·42	0·11	0·12	1·16	0·12	0·12	1·20	0·08	0·18	0·12	18·14	0·23	0·26	[19·30	0·24	0·24
5·33E	0·25	0·14	0·15	0·92	0·16	0·15	0·93	0·11	0·17	0·15	18·87	0·32	0·36	19·79	0·31	0.31
6·00E	0·28	0·14	0·15	1·01	0·16	0·15	0·96	0·11	0·17	[0·15	18·82	0·31	0·35	19·83	0·31	0·31

6·67E	0·22	0·16	0·17	1·08	0·17	0·16	0·98	0·12	0·16	0·17	18·95	0·33	0·37	20·03	0·34	0.34
7·33E				0·79	0·21	0·20	1·19	0·14	0·15	0·21	19·62	0·45	0·51	20·41	0·41	0·41
8·00E				1·42	0·24	0·22	1·18	0·16	0·47	0·23	19·28	0·38	0·43	20·70	0·46	0·46
8·67E				1·71	0·32	0·30	1.16	0·22	0·37	0·31	19·63	0·45	0·51	21·34	0·62	0·62
9·33E							1·29		0·15		20·32	0·62	0·68			
							North-South scan									
9·5N				0·07	0·03	0·03	0·23	0·02	0·13	0·03	16·21	0·09	0·10	16·28	0·06	0·06
8·5N				1·10	0·22	0·21	0·88	0·15	0·15	0·22	19·43	0·41	0·47	20·53	0·43	0·43
7·5N				1·50	0·31	0·29	0·76	0·21	0·13	0·30	19·77	0·48	0·55	21·27	0·60	0·60
6·5N				1·24	0·19	0·20	0·93	0·15	0·56	0·21	19·26	0·38	0·43	20·50	0·42	0·42
4·5N	0·35	0·10	0·11	0·89	0·11	0·10	0·92	0·07	0·07	0·11	18·13	0·23	0·26	19·02	0·21	0·21
3·5N	0·32	0·08	0·09	0·85	0·11	0·09	0·90	0·06	0·07	0·09	17·79	0·19	0·44	18·64	0·18	0·18
2·5N	0·23	0·06	0·06	0·90	0·06	0·06	1·00	0·05	0·38	0·07	17·11	0·14	0·16	18·01	0·13	0·13
1·5N	0·12	0·06	0·06	0·83	0·06	0·06	0·90	0·05	0·36	0·07	17·03	0·14	0·16	17·86	0·13	0·13
0·5N	0·16	0·05	0·05	0·90	0·05	0·05	0·99	0·04	0·52	0·06	16·64	0·11	0·13	17·54	0·11	0·11
0·5S	0·21	0·06	0·06	0·88	0·05	0·05	0·97	0·04	0·50	0·06	16·85	0·13	0·15	17·73	0·12	0·12
1·5S	0·29	0·06	0·06	0·95	0·06	0·06	1·01	0·05	0·38	0·07	17·06	0·14	0·16	18·01	0·13	0·13
2·5S	0·33	0·07	0·07	0·96	0·08	0·08	1·04	0·06	0·27	0·08	17·36	0·16	0·18	18·32	0·16	0·16
3·5S	0.22	0·11	0·12	0·94	0·12	0·11	0·98	0·08	0·21	0·12	18·21	0·23	0·26	19·15	0·23	0·23
4·5S	0·22	0·11	0·12	1·21	0·12	0·11	1·10	0·08	0·23	0·12	18·01	0·21	0·24	19·22	0·23	0·23
5·5S	0·33	0·15	0·16	1·08	0·17	0·16	0·93	0·12	0·30	0·17	18·89	0·32	0·36	19·97	0·33	0·33
6·5S	0·22	0·18	0·19	1·13	0·20	0·19	0·97	0·14	0·07	0·20	19·19	0·37	0·42	20·32	0·39	0·39
7·5S	0·50	0·26	0·28	1·67	0·29	0·27	1·33	0·20	0·25	0·28	19·45	0·41	0·47	21·12	0·56	0·56
8·5S				1·77	0·33	0·31	1·07	0·23	0·11	0·33	19·67	0·46	0·52	21·44	0·65	0·65
9·5S				2·35	0·48	0·45	1·08	0·33	0·27	0·47	19·89	0·51	0·58	22·24	0·94	0·94
10·5S				1·71	0·39	0·37	0·83	0·27	0·00	0·39	20·09	0·56	0·64	21·80	0·77	0·77

from the M 3 model. In columns 4, 7, 9, 11, 14 and 17, we have listed the sampling errors in $U - B$, $B - V$, $V - R$, $R - I$ colours and V, B bands respectively, as derived from the M 92 model.

We find that the sampling errors obtained from both the models are comparable. Sampling errors for the region within 4 arcmin from the centre of the cluster vary from 0·06 mag to 0·09 mag. Since the colour is symmetric with respect to the centre of the cluster, this value may be divided by $\sqrt{2}$ and hence the average sampling error in this region is of the order of 0·05 mag.

Fig. 1 shows the variation of colours $U - B$, $B - V$, $V - R$ and $R - I$ and the brightness in V along both the east-west and north-south directions. In Fig. 2 we plot the individual V magnitudes and $B - V$ colours in the east-west direction obtained on two consecutive nights. These points indicate the reproducibility of our measurement from night to night. The bumps in the wings of the brightness profile are inherent in the cluster. Similar bumps have been seen by Gascoigne and Burr (1956) for both ω Cen and 47 Tuc. Such abrupt changes in intensity are often asso-

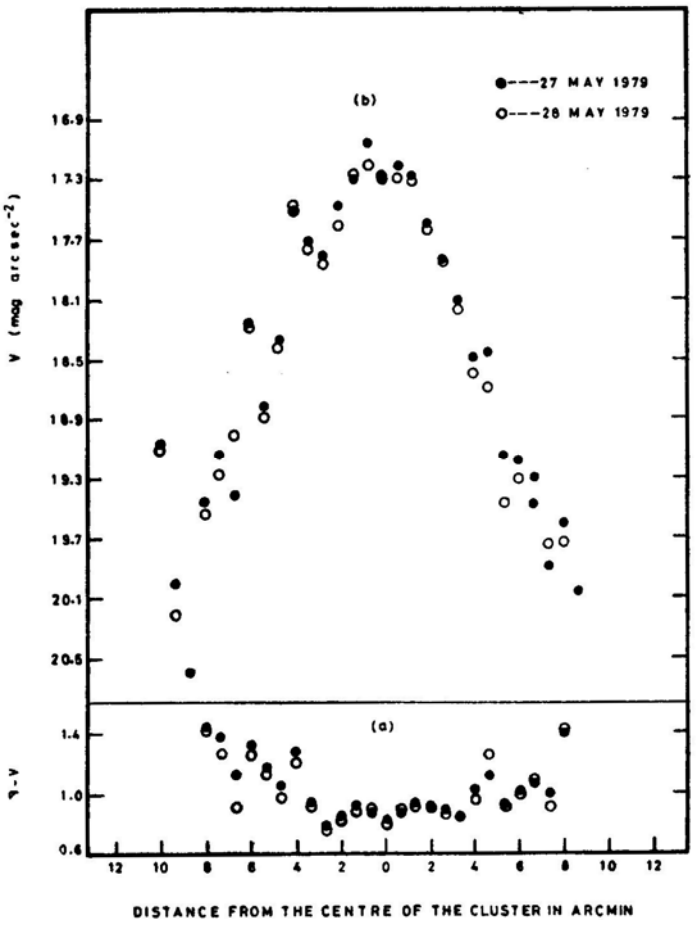

Figure 2. V magnitudes and $B - V$ colours obtained on two consecutive nights by an aperture scan of ω Cen in the east-west direction. The stability of the counts proves the accuracy of positioning the aperture over the cluster.

Table 3. Log f values for the two scan directions.

East-West Scan						North-South Scan					
log r	log f					log r	log f				
	U	B	V	R	I		U	B	V	R	I
−0·176	−3·116	−3·048	−2·692	−2·296	−2·100	−0·303	−3·116	−3·044	−2·688	−2·296	−2·092
0·125	−3·195	−3·103	−2·739	−2·335	−2·160	0·176	−3·251	−3·171	−2·815	−2·431	−2·283
0·301	−3·294	−3·206	−2·854	−2·462	−2·330	0·398	−3·378	−3·262	−2·894	−2·482	−2·354
0·426	−3·383	−3·287	−2·961	−2·591	−2·500	0·544	−3·663	−3·559	−3·199	−2·823	−2·767
0·523	−3·480	−3·360	−3·004	−2·624	−2·520	0·653	−3·760	−3·648	−3·228	−2·824	−2·764
0·602	−3·637	−3·477	−3·027	−2·589	−2·453	0·740	−4·121	−3·989	−3·557	−3·185	−3·065
0·669	−3·813	−3·657	−3·219	−2·785	−2·705	0·813	−4·217	−4·165	−3·689	−3·309	−3·185
0·727	−4·037	−3·873	−3·457	−3·053	−2·977	0·875	−4·649	−4·477	−3·845	−3·625	−3·549
0·778	−4·017	−3·797	−3·333	−2·901	−2·813	0·929		−4·597	−3·821	−3·429	−3·381
0·824	−4·160	−3·968	−3·546	−3·108	−3·012	0·978		−4·897	−3·956	−3·524	−3·417
0·865	−4·344	−4·100	−3·676	−3·184	−3·092	1·021		−4·720	−4·036	−3·704	−3·704
0·903		−4·236	−3·668	−3·164	−3·008						
0·938		−4·536	−3·972	−3·388	−3·176						
0·970			−3·998	−3·448	−3·332						

ciated with changes in colour. The bumps are barely noticeable in a U scan; they are striking in either R or I. Table 3 gives the mean surface brightness log f in the U, B, V, R and I bands expressed in units of 10·0 mag arcsec^{-2}. Column 1 gives log r where r is the distance from the centre in arcmin. Columns 2, 3, 4, 5 and 6 give the values of log f in the U, B, V, R and I bands. These are the means around the centre, separately evaluated for the east-west and the north-south scans. In evaluating the mean variation of surface brightness, the values at the locations of bumps in the profile have not been included. The log f values given here have been corrected for aperture smoothing, using an approximate equation similar to the one used by Illingworth and Illingworth (1976) for concentric aperture measures. In Fig. 3, we have plotted log f against log r (r in arcmin) along the major axis for the U, B, V, R and I bands. For the V band, the measures of Gascoigne and Burr as well as those of Da Costa (1979) uncorrected for the ellipticity of the cluster, are also plotted together with our results. The plot gives the values of log f_0 = 2·700 where f_0 is the surface brightness at r = 0 (King 1962) and is expressed in units of V = 10·0 mag arcsec^{-2}. From the measured U — B, B — V, V — R and R — I colours for the centre of the

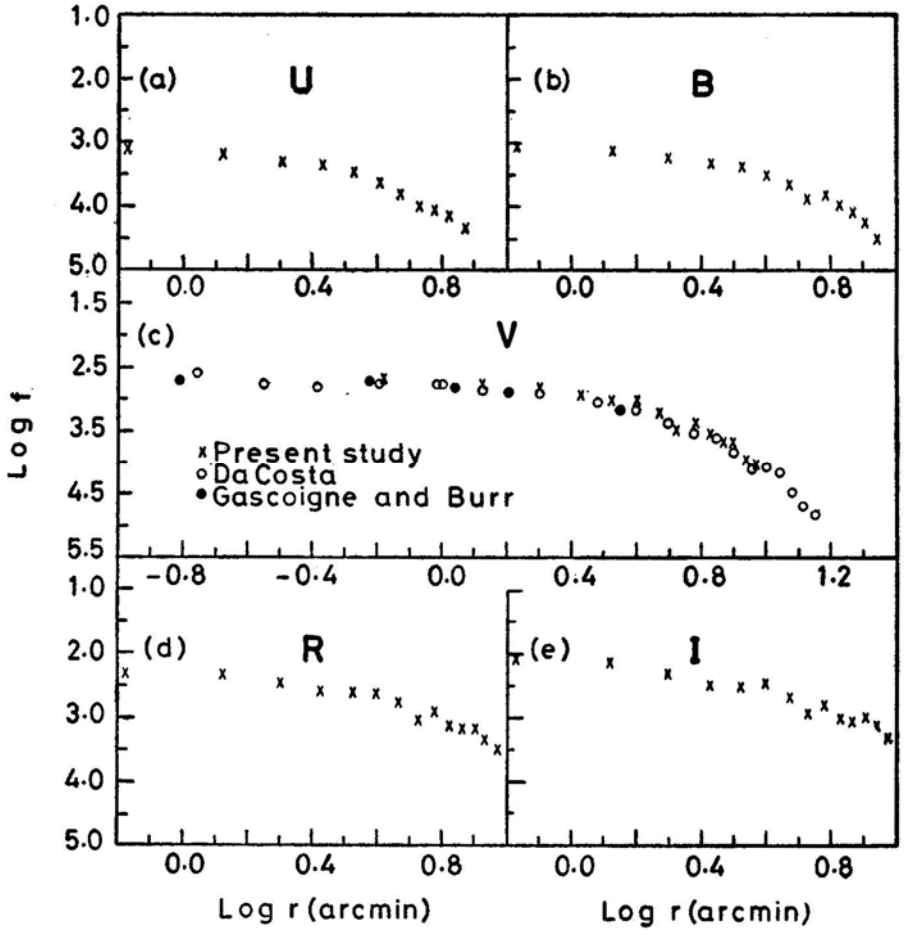

Figure 3. Variation of surface brightness over the cluster ω Centauri in U, B, V, R and I bands in the direction of the major axis. The central frame (c) has the measures of Gascoigne and Burr (1956), Da Costa (1979) as well as the results of the present study for the V band.

cluster, we have calculated the values of log f_0 for the remaining wavelength bands. Table 4 gives the mean values of cluster brightness and colour at the centre in the U, B, V, R and I bands.

The variation of log f with distance from the centre of the cluster along both the major and minor axes is shown in Fig. 4 for the five wavelength bands of observation. The continuous lines in each figure show the best fitting model of King (1966a).

Table 4. log f_0 values for different wavelength bands.

Wavelength band	log f_0
U	−3·112
B	−3·048
V	−2·700
R	−2·312
I	−2·128

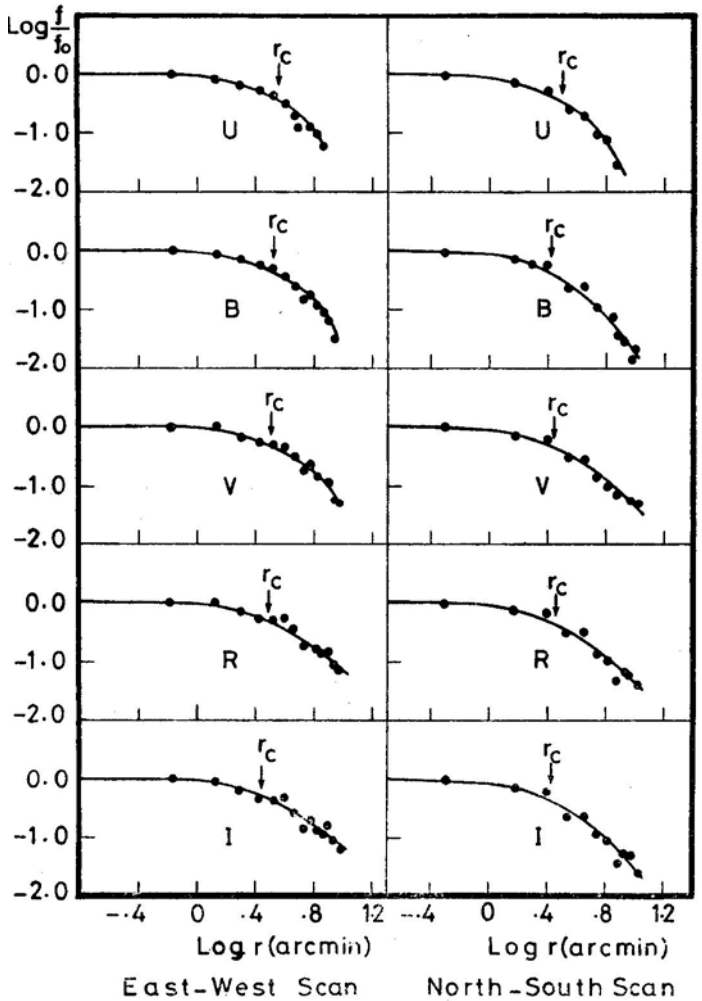

Figure 4. Surface brightness profiles in *U*, *B*, *V*, *R* and *I* bands, of ω Cen, along the major and minor axes. Continuous lines in each figure show the best fitting model of King (1966a). Core radii r_c are marked.

The core radius r_c and the concentration factor $C = \log (r_t / r_c)$ for the curves fitted to the five wavelength bands are given in Table 5. The last column in Table 5 gives the ratio of the core radius along the minor axis to that along the major axis, in the respective bands. Three aspects of the colour variation over the cluster are of interest. These are the dependence of the cluster ellipticity, the derived core radii and the values

Table 5. Core radii and concentration factors for different wavelength bands.

Wavelength band	East-West scan		North-South scan		$\frac{r_c \text{ (minor)}}{r_c \text{ (major)}}$
	$\log r_c$	$\log (r_t/r_c)$	$\log r_c$	$\log (r_t/r_c)$	
U	0·55	0·75	0·50	0·75	0·89
B	0·52	1·00	0·42	1·00	0·79
V	0·50	1·25	0·44	1·25	0·87
R	0·48	1·50	0·45	1·25	0·93
I	0·44	1·75	0·42	1·25	0.96

of the concentration factor on wavelength. The cluster appears more elliptical in the short wavelength bands than at the longer wavelengths. The values of core radii are greater in the ultraviolet or blue than in the red and near infrared. If the distribution of blue star experiences a peak, before it falls with increasing radial distance from the centre, the contribution of these stars to the intensity in the blue will be such as to give a larger value of the core radius. It is of interest to recall that Dickens and Woolley (1967) have observed a larger concentration of bright horizontal branch (HB) stars in the major axis sectors than in the minor axis sectors. This is further corroborated by the study of Strom, Strom and Goad (1976) who have observed colour gradients in E and S0 galaxies to be the greatest along the minor axis. As seen in a later section of this paper our counts of HB stars show a preponderance along the major axis than in a direction perpendicular to it. This feature also explains how the values of r_c along the minor axis do not show a striking dependence on colour. The variation in radial gradient of the blue component of stars along the minor axis is insufficient to modify the light distribution significantly. Also, the values of the concentration factor (C) show a gradual increase from short wavelength bands to the long wavelength bands. This could be because of a faster decrease of the number density of the stars contributing to the surface brightness in the blue band compared to that of the red stars which contribute most of the light in the I band. The core radius and the concentration factor C obtained by us in the visual band are comparable in magnitude to the values obtained by King (1966a) and Da Costa (1979), even though the technique employed is different and the data covers only a limited region of the cluster.

Fig. 5 shows the distribution of $B - I$ colour along the major and minor axes. The curve is fairly symmetrical around the centre. The region between A_1 and A_2 has a diameter of about 3·5 arcmin with $B - I \simeq 2{\cdot}45$ mag. Beyond this region the cluster gets bluer and reaches a maximum blueness at B_1 and B_2. The difference in $B - I$ colour between the centre and this zone is 0·45 mag. The width of this zone is about 1·5 arcmin. Beyond B_1, B_2 the cluster becomes redder again. The change in colour is rather sharp. The arrows in the figure show the regions where the cluster has a discontinuity in the trend. The effect of these three zones on the equidensity contours is discussed later.

Fig. 6(a) shows the ($U - B$, $B - V$) relation for the observed regions of the cluster.

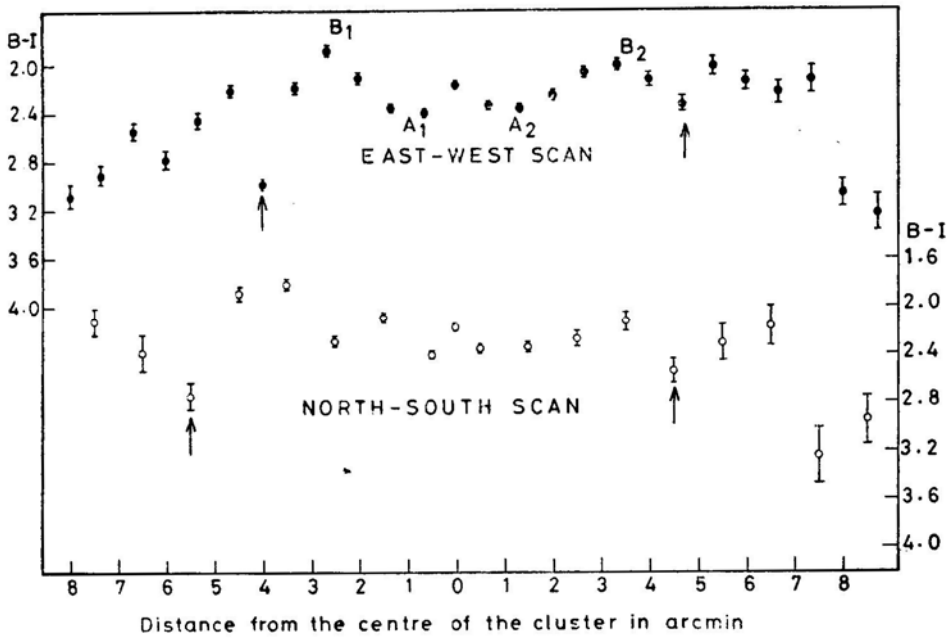

Figure 5. Distribution of B — I colour along the major and minor axes of ω Cen. The scale for the east-west (major axis) scan is at the left while the scale at the right corresponds to the north-south (minor axis) scan.

The points on the minor and major axes can be easily discerned. A number adjacent to each point indicates its distance in minutes of arc from the cluster centre. The continuous line is the intrinsic (U — B, B — V) relation (Eggen and Sandage 1965) for the main sequence, shifted by E_{B-V} = 0·11 mag and E_{U-B} = 0·08 mag for space reddening. In Fig. 6(b) we have plotted the values of δ (U — B), the ultraviolet(UV) excess, for each point. This excess is the difference between the Hyades standard relation and the observed U — B for each observed B — V point. The abscissa shows the distance r of the point from the cluster centre. We note that from r = 0 to r = 1·7 arcmin the UV excess values range between 0·2 and 0·3 mag. Of considerable intererst is the fact that the UV excess right at the centre is only 0·2 mag. Beyond r = 4 arcmin, the UV excess keeps increasing with increasing distance from the cluster centre. Between r = 1·7 arcmin and r = 4 arcmin, the UV excess shows a decrease with a minimum value around 3 arcmin. This is also the region where the cluster has become bluer in B — I by about 0·45 mag over its value at the cluster centre.

The presence of a large number of red stars around the cluster has been observed by Dickens and Woolley (1967). The total counts for the region from 3·5 arcmin to 5·5 arcmin from the cluster centre, are 917 for the red and 298 for the blue stars. Most of these red stars are much brighter than the blue stars in the cluster and hence the contribution to surface brightness by these red stars is much more than what the counts show. The kinks seen in the B — I versus r curve located in Fig. 5 by arrows, are the result of the presence of these red stars. Almost all the globular clusters observed by Strauss (1978) show similar kinks in B — I colour. The stars at the centre and the stars that give rise to the kinks have similar B — I colours and UV excesses. The

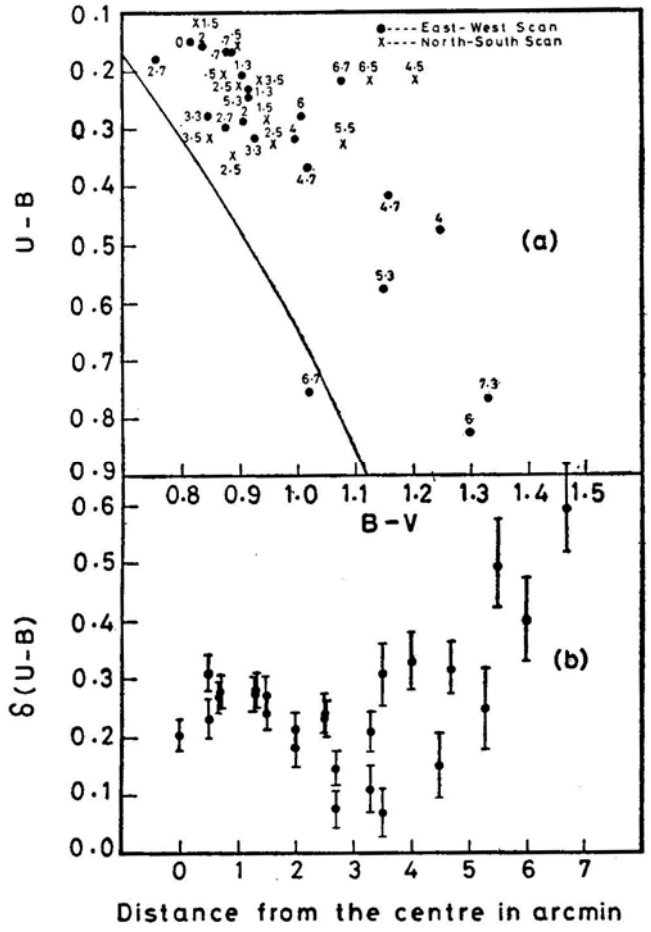

Figure 6. (a) U — B, B — V relation for the observed regions of the cluster ω Cen. The number marked against each point is the distance in minutes of arc from the centre of the cluster. (b) The dependence of the UV excess of these regions on their distance from the centre. The sampling error in U — B is shown by vertical bars.

zone between these two regions is different in that it has a bluer colour and a smaller UV excess.

Three colour photometry by Sandage and Walker (1966) on M 92 shows that the stars belonging to the subgiant sequence can be separated from the asymptotic giant branch (AGB) stars in a (U — B, B — V) diagram. *UBV* photometry on M 3 by Johnson and Sandage (1956) and on ω Cen by Geyer (1967) show the same effect. But this photometric difference is not seen in the spectral features of the stars belonging to these groups. A moderate resolution spectrophotometric survey of M 92 by Strom and Strom (1971) revealed no difference in the spectral energy distribution except for wavelengths below the Balmer jump. Strom and Strom find that the differences in δ (U — B) between the red giants and the AGB stars have a weak dependence on distance of the star from the cluster centre. For the red giants in M 92, they get a UV excess of 0·24 mag. This matches well with our value of 0·26 mag for the region around the centre of ω Cen. Strom and Strom also get a UV excess value of 0·04 mag for the AGB stars which compares well with our value of 0·10 for the

intermediate region in the cluster ω Cen. Any attempt to seek a one-to-one correspondence between the $\delta(U - B)$ behaviour of individual stars and that in the integrated light of the different regions of the cluster, is perhaps not justified because of the contribution of the blue horizontal branch (BHB) stars to the *UBV* light of the cluster. But the similarity in the range of $\delta(U - B)$ values gives an indication of the kind of stars which dominate the surface brightness in any of the different regions of the cluster studied.

We now search for a similar distance dependence of UV excess in M 3 from published data by Sandage (1953). Stars measured by him from Series I plates cover a magnitude range of $12{\cdot}7 \leqslant m_{\dot{y}} \leqslant 17{\cdot}5$ and are selected from an annulus with the inner and outer radii of 100 arcsec and 600 arcsec respectively. In Fig. 7 we have plotted the UV excess of these stars against their distance from the cluster centre. Stars which belong to the giant branch, subgiant branch, horizontal branch, asymptotic giant branch and the blue extension of the horizontal branch are plotted with different symbols in the figure. All the stars measured within 2·75 arcmin from the centre of the cluster show UV excess much lower than what is seen outside this zone. It is apparent that all stars located within 2·75 arcmin of the cluster centre have small values of UV excess, regardless of their position in the HR diagram. The giant branch (GB) stars have large UV excess only when they are located outside the 2·75 arcmin zone. The AGB stars for which the photometric data are available fall within the 2·75 arcmin zone and show small UV excess. The BHB stars are the stars with a UV deficit and these are within the 2·75 arcmin zone. The range in δ $(U - B)$ is very large for the giants. The BHB stars in the cluster form a homogeneous group having similar brightness and colour. If we consider the mean UV excess of the BHB stars within 2·75 arcmin from the cluster centre and also outside 2·75 arcmin from the centre, we find that the BHB stars in the inner region have UV excess smaller by 0·05 mag when compared to the UV excess of BHB stars in the outer region. This difference in UV excess should be definitely coming from a diffuse background radiation, affecting the photometry of individual stars. The fact that the BHB stars nearer to the centre have a smaller UV excess when compared to the outer stars, shows the similarity of the radiation from the BHB stars and the diffuse background.

The small UV excess in the intermediate region in ω Cen can be due to (i) the contribution from a diffuse background which has properties similar to the HB stars, (ii) an increase in the number density of HB stars and (iii) a decrease in the number of bright red giants. The results of the photometry of individual stars in M 92 and M 3 show the effect of the background on the UV excess of the stars very clearly. The increase in the density of HB stars in the intermediate region of the cluster ω Cen (from 1·7 arcmin to 4 arcmin) and also its correlation with the ellipticity derived from equidensity contours of the cluster are demonstrated in a later section. A region with numerous HB stars will therefore show, in integrated light, the effects of a small UV excess. The core of the cluster is abundant in closely packed bright red stars and hence the disturbing effects of the radiation from the diffuse background and HB stars are not very apparent. Right at the centre there is a zone of 40 arcsec diameter where the bright red stars are few; this region is found to show a smaller UV excess as seen in Fig. 6. There is an increase in the number of HB stars with increasing distance from the centre. This results in a bluer colour and smaller UV excess in integrated light that originates from the intermediate zone in ω Cen.

Wherever the aperture comes across bright red stars during the scan, 'kinks' are produced in the colour curve as seen in Fig. 5 and 'bumps' in the surface brightness profiles as seen in Fig. 1. Gascoigne and Burr (1956) have shown that these bumps are seen not only in the profiles of ω Cen on both sides of the cluster centre, but also in 47 Tue at a distance of about 2 to 2·5 arcmin from the centre. This becomes significant when we consider the fact that 47 Tuc also becomes bluer beyond 2 arcmin from the centre.

A large range in δ (U — B) for the giant branch and the main sequence stars of M 3 has been pointed out by Johnson and Sandage (1956). Despite the scatter in these values, as seen in Fig. 7, at large distances from the cluster centre, the dependence of δ (U — B) on distance from the centre is obvious and this aspect seems best ascribed to a background contribution similar to the BHB stars of low UV excess.

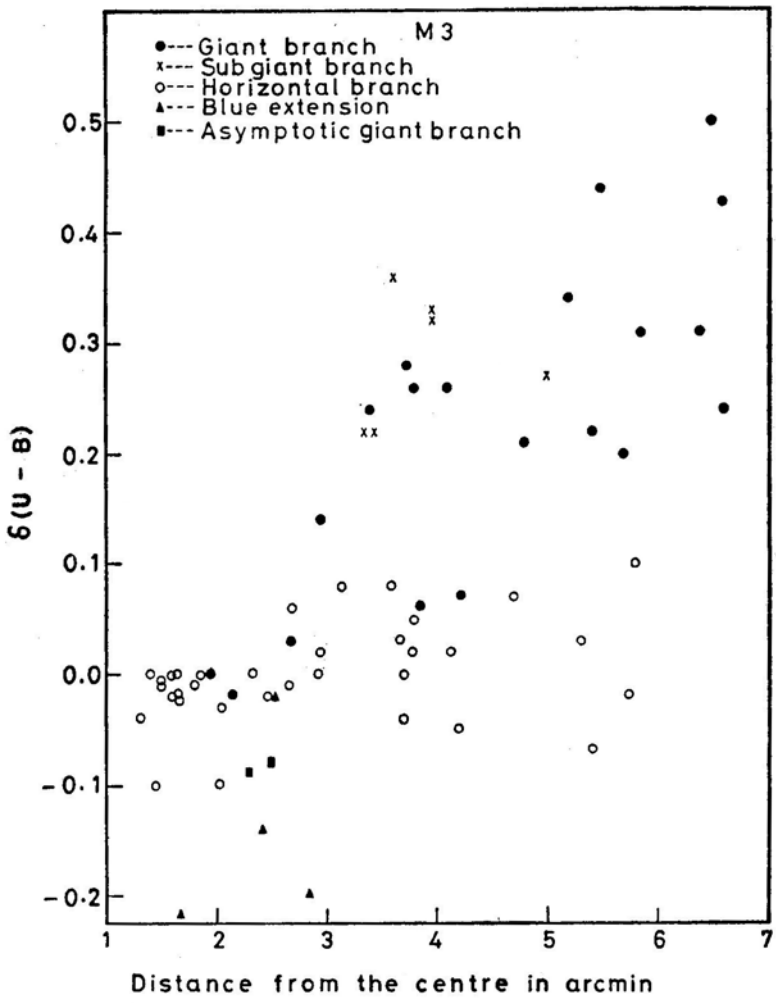

Figure 7. Plot of UV excess δ (U — B) of stars in M 3 measured by Sandage (1953) from series I plates, against the distance from the centre. The effect of the blue diffuse background is found to be maximum within 2.75 arcmin from the centre.

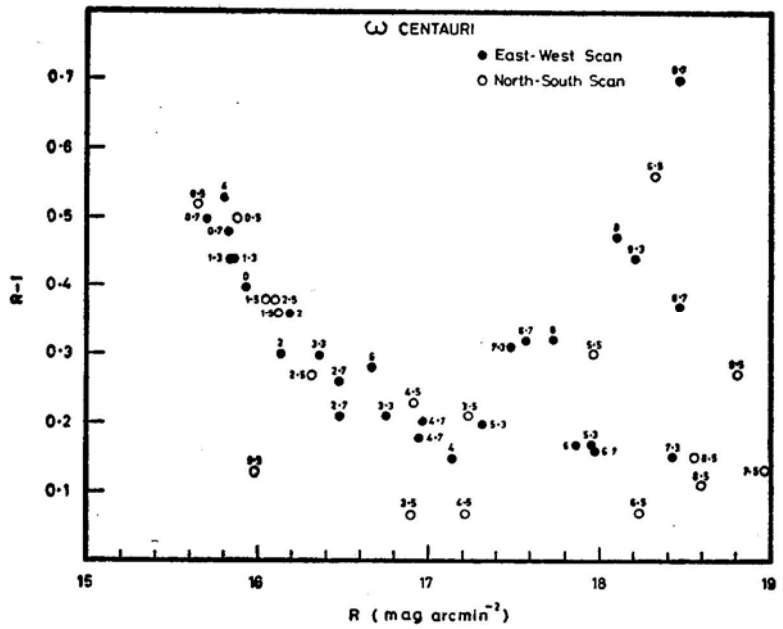

Figure 8. *R*, *R* — *I* relation for the observed regions of the cluster ω Cen. The number marked against each point shows the distance from the centre in minutes of arc.

2.4 *R*, *R*– *I Relation*

Fig. 8 is a plot of *R*, the surface brightness in mag arcsec^{-2} against *R* — *I* colour over the cluster ω Cen along the major and minor axes. Major axis locations are shown by filled circles and those on the minor axis by open circles. The number marked near each point shows its distance from the centre of the cluster in minutes of arc. The diagram shows the cluster to be the reddest near the centre, and becoming blue away from the centre. Since the contribution to the surface brightness of the red stars is decreasing and that from the bluer stars is increasing we can expect to see the colour of the cluster becoming bluer as we go outwards from the centre with normalcy in redness restored in the outer regions. The change appears to be the same for the major and minor axes. The large scatter at faint values of brightness can be caused by the sporadic appearance within the diaphragm of a red or blue star either belonging to the cluster or to the background field. Of particular interest is the fact that right at the centre the cluster is bluer than the region at its immediate vicinity (0·5 arcmin away). This aspect is also similar to the pattern seen in the $\delta(U — B)$ variation.

In the next section, we will show how this change in the distribution of colour affects the equidensity contours of the cluster.

3. Equidensitometry of ω Centauri and 47 Tucanae

Aperture photometry carried out by us and the photometric observations of individual stars made by other authors show an increase in the population of giants towards the

centre of ω Cen. We have seen in an earlier section, evidence for a blue bulge of resolved and unresolved stars around the central regions. The effect of this peculiar distribution of blue and red stars will be apparent in the results of multicolour equidensitometry of the cluster. The segregation effects are best seen in the dense inner regions of the cluster. In these regions of high star density, only equidensitometry can be used to study the ellipticity and colour gradients. We have used the well known Sabattier technique to obtain equidensity contours of the cluster. The Sabattier technique has been employed earlier on globular clusters, for a determination of the axial ratios and the position angles of the major axes. Kadla (1966) and Sistero and Fourcade (1970) used the technique with success on M 13 and ω Cen respectively. These results on the degree of ellipticity of the two clusters are in conformity with the results of star counts. Kadla *et al.* (1976) made a detailed study of the dependence of the axial ratio b/a and the position angle of the major axis, on the distance from the centre of the clusters M 3, M 5, M 13, M 15 and M 92 in *UBV* and *R* bands. In all these clusters the ellipticity reaches a maximum at a certain distance from the cluster centre, depending on the cluster. In some clusters like M 92 and M 5, the curves show well defined regions of minimum ellipticity close to the centre and again at some distance away from the cluster centre. The position angle of the major axis of this inner region is, however, different from that of the outer region in both these clusters.

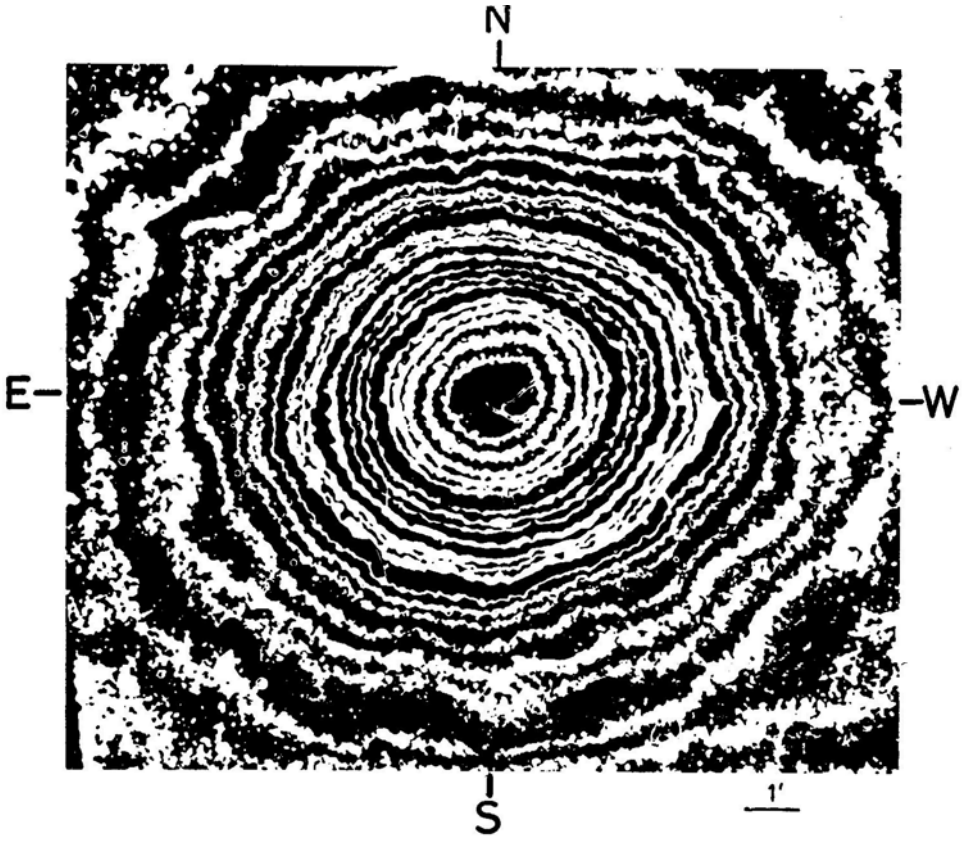

Figure 9. Equidensity contours of ω Cen in the *V* band.

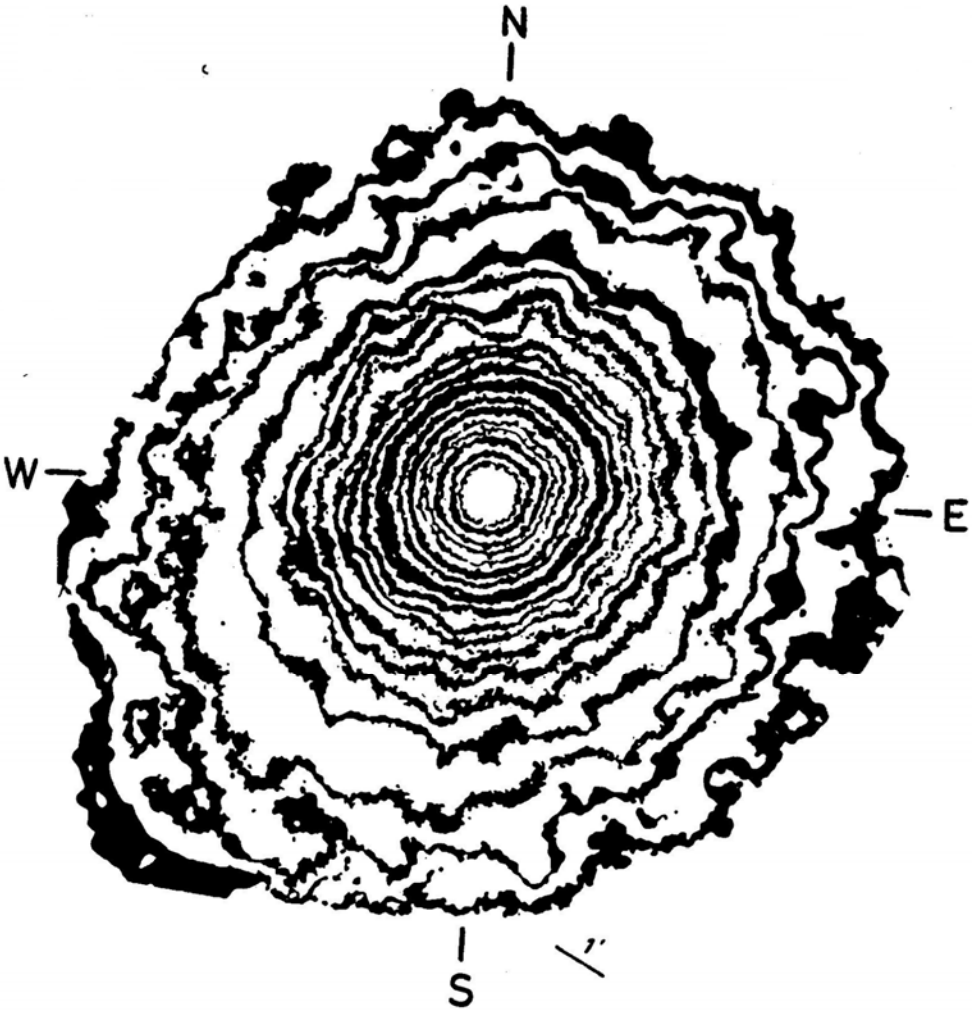

Figure 10. Equidensity contours of 47 Tuc in the *V* band.

3.1 *The Equidensity Contours*

We have derived equidensity contours of ω Cen from photographs taken through the filter and emulsion combinations of the standard *B*, *V* system, together with an infrared band isolated by the combination of hypersensitized I-N and an RG 8 filter. The equidensity contours of 47 Tuc were also obtained from a *V* photograph kindly supplied by Dr Martha Liller. A diffuser was introduced between the photographic film and the cluster photograph while taking the initial graded exposures. Outlying stars on the plate are used to match the contours while making the isophote maps. Equidensity contours of ω Cen and 47 Tuc in *V* band are shown in Figs 9 and 10 respectively. For each contour, we have measured *x*, *y* coordinates for 72 points on the contour at 5° intervals along with the *x*, *y* coordinates of 2 reference stars of the cluster. A computer program is used to derive the axial ratio *b/a*, position angle ϕ,

area within each contour, (x, y) coordinates of the centre of each contour and the respective errors. The origin of the coordinate system is the star marked T in Fig. 14 and the x-axis is the line joining T to the second reference star M. Since all the distances are normalised to the distance TM on every plate, the small differences in the scales of the plates taken in B, V and infrared bands will not cause any error in the results. Detailed measures are published elsewhere (Scaria 1980).

In Fig. 11(d) we note the change of axial ratios with distance from the centre in the B and the infrared bands. The contour 1·7 arcmin distant from the centre along the major axis is the closest to a circle in shape. Beyond this location the ellipticity increases and reaches a maximum around 3 arcmin from the centre. As one continues outward, the ellipticity decreases to a minimum given by an axial ratio of 0·88 before

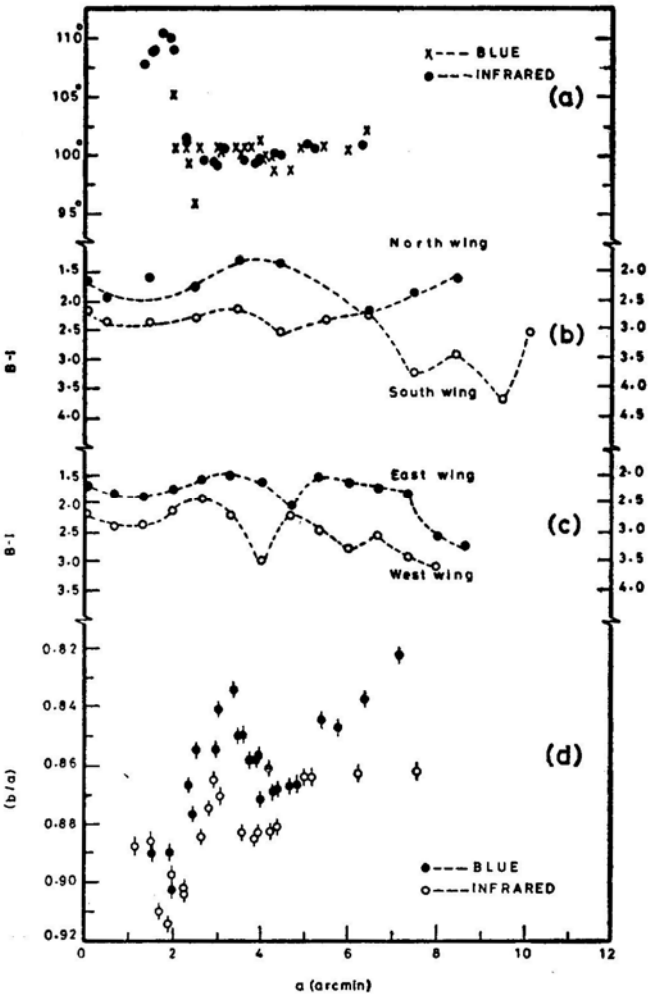

Figure 11. (a) The variation of position angle of the major axis of the equidensity contours of ω Cen as a function of the semi major axis (a). (b) The variation of B — I colour along the minor axis of ω Cen. The north wing (scale at right) and the south wing (scale at left) are separately shown. (c) The variation of B — I colour along the major axis of ω Cen. The east wing (scale at right) and the west wing (scale at left) are separately shown. (d) The variation of the axial ratio (b/a) of the equidensity contours of ω Cen as a function of the semimajor axis (a).

it increases again in the outermost regions. It should be noted that the cluster is definitely less elliptical in the infrared band than it is in the blue band. This difference is very pronounced everywhere beyond 2 arcmin from the centre. We plot in Fig. 11 (a) the position angle ϕ against a the semimajor axis. A change in position angle is quite striking between 1·7 arcmin and 2·5 arcmin. Beyond this there is little change in the outer regions.

Fig. 12 is a plot of b/a against a for the clusters M 92 and ω Cen in the B band. Data for M 92 is taken from Högner *et al.* (1973). The values of a for M 92 have been normalized to the distance of ω Cen. The great similarity between the two curves shows that whatever dynamical conditions prevail in ω Cen are also found in M 92. Plots of similar data for M 5 obtained by Kadla *et al.* (1976) are also alike. All these clusters show a minimum in b/a at 3·2 arcmin from the centre, with low values appearing again in the outer regions. There is also a sudden change in the position angle of the major axis in the vicinity of the location of the first minimum.

Figs 11 (b) and (c) show the change in the B — I colour across the cluster. The B — I colour along the east, west, north and south wings are plotted separately. The most striking feature in the figure is that the change in ellipticity is connected with a change in colour. The core, which can be identified in the colour curve, matches with the first minimum in ellipticity. As we go outwards, we come across the bluer region in the cluster where the ellipticity reaches the highest value seen in the cluster. The

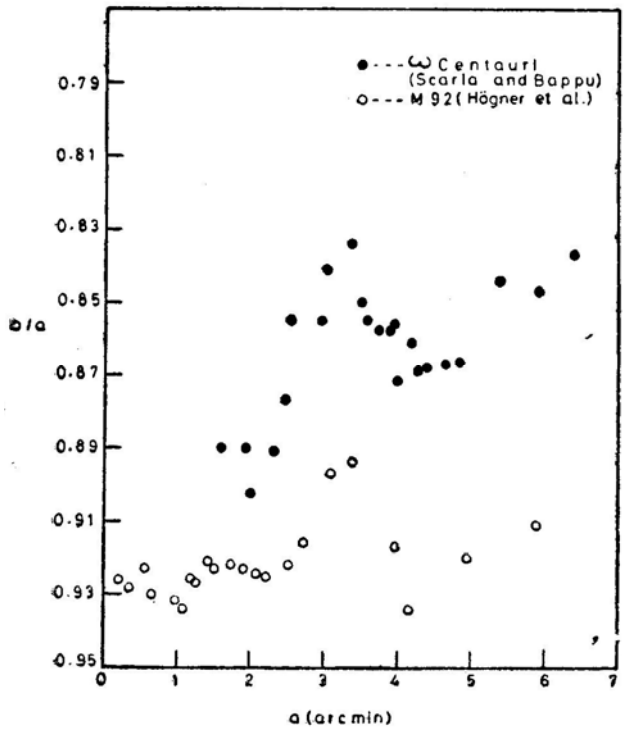

Figure 12. The relationship between b/a and a for the clusters ω Cen and M 92. Values of semimajor axis a for M 92 have been normalized to the distance of ω Cen. The data for M 92 is taken from Högner *et al*. (1973).

second minimum in the ellipticity curve falls in the region of the colour curve where the cluster is becoming redder with distance from the centre. This is the region where Dickens and Woolley (1967) get larger counts for red stars as compared to the blue ones. Thus, wherever the red stars predominate, the cluster ellipticity is small. The blue stars appear as a bulge around the core and this system shows a distribution more elliptical than the system of red stars. This blue bulge is between 1·7 arcmin and 4·0 arcmin from the centre.

Fig. 13 shows the relationship between the ellipticity curve and the colour curve of 47 Tuc. The colour curve is obtained from the photometry of Chun and Freeman (1979). The ellipticity curve was obtained by us in the V band through the same procedure as explained earlier. Our conclusion that the cluster ellipticity increases where the cluster is becoming bluer, is found to be valid here also. The diaphragm used by Chun and Freeman is too large to demonstrate strikingly a differential colour

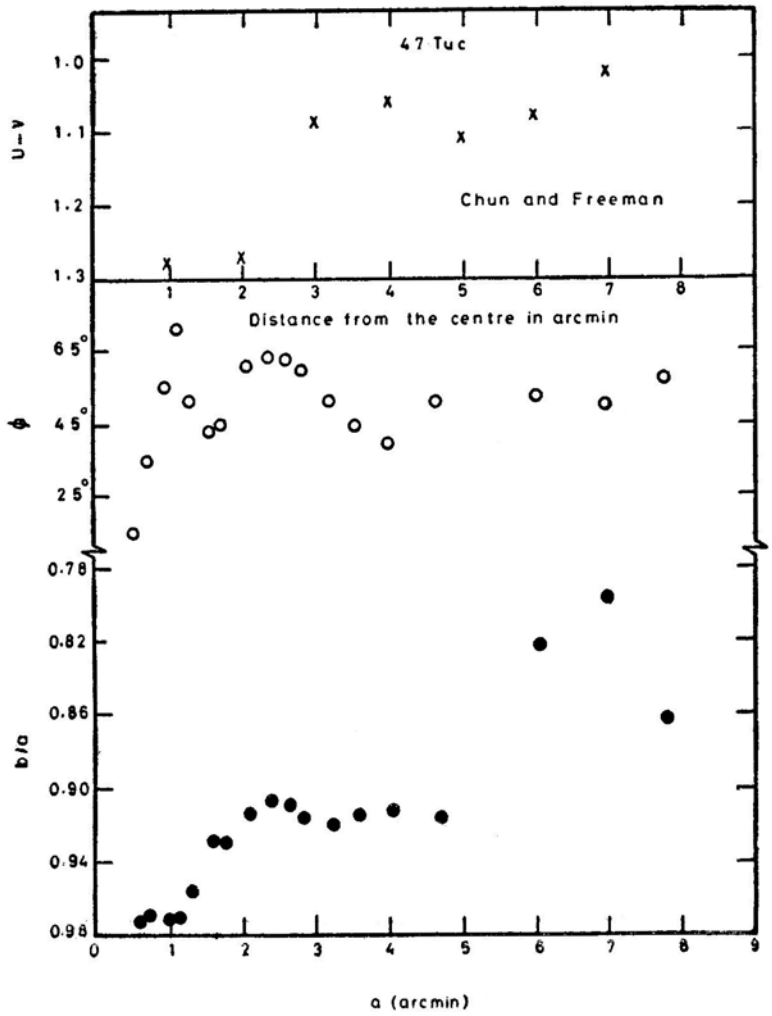

Figure 13. Variation of $U - V$ colour, position angle of the major axis (ϕ) and the ellipticity (b/a) for the cluster 47 Tuc as a function of distance from the centre.

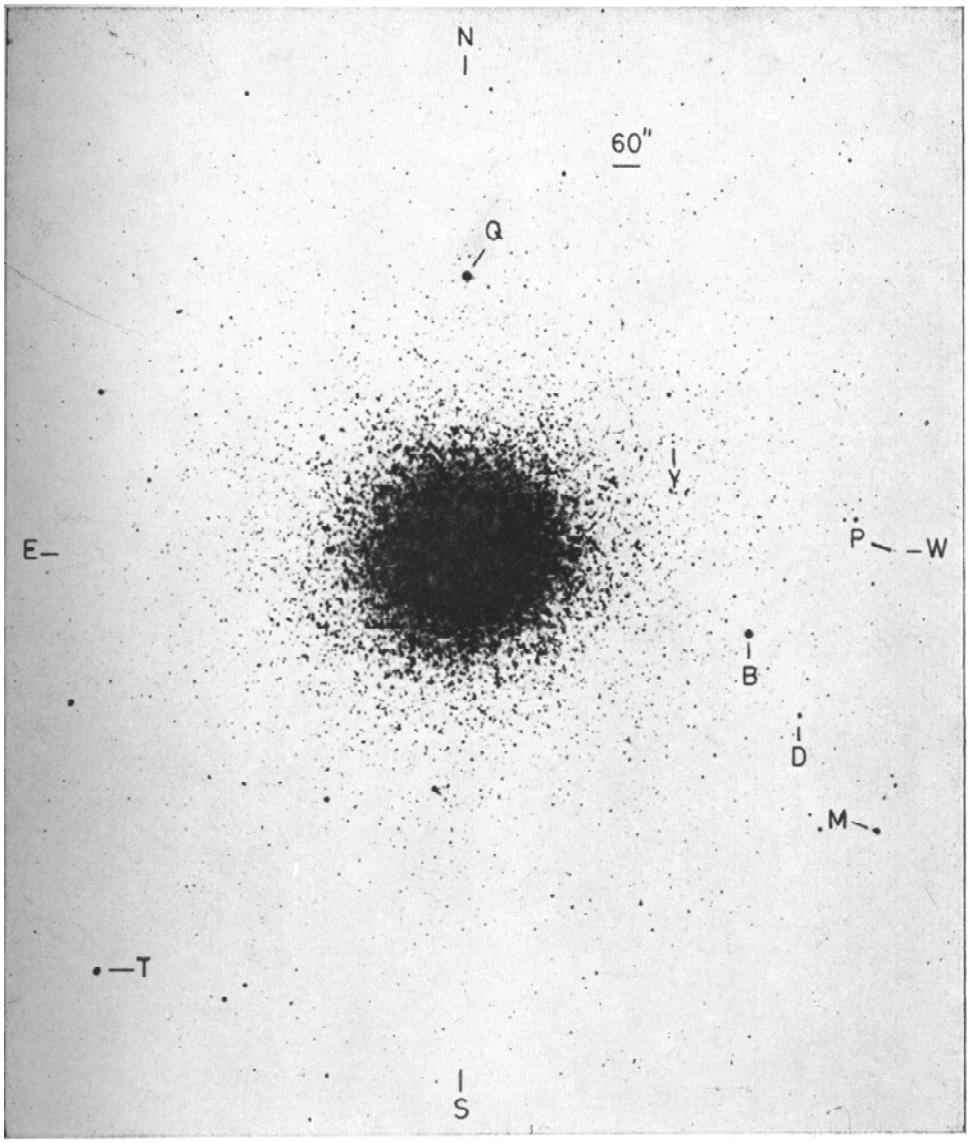

Figure 14. ω Cen in *B* band taken with the 102-cm reflector at Kavalur. Stars marked T and M are the reference stars for the equidensitometry of the cluster. Star P is the reference star for the scan in the east- west direction and star Q is the reference star for the north-south scan. Stars B and D are the two photoelectric standards. Star Y has been identified in Fig. 15(b).

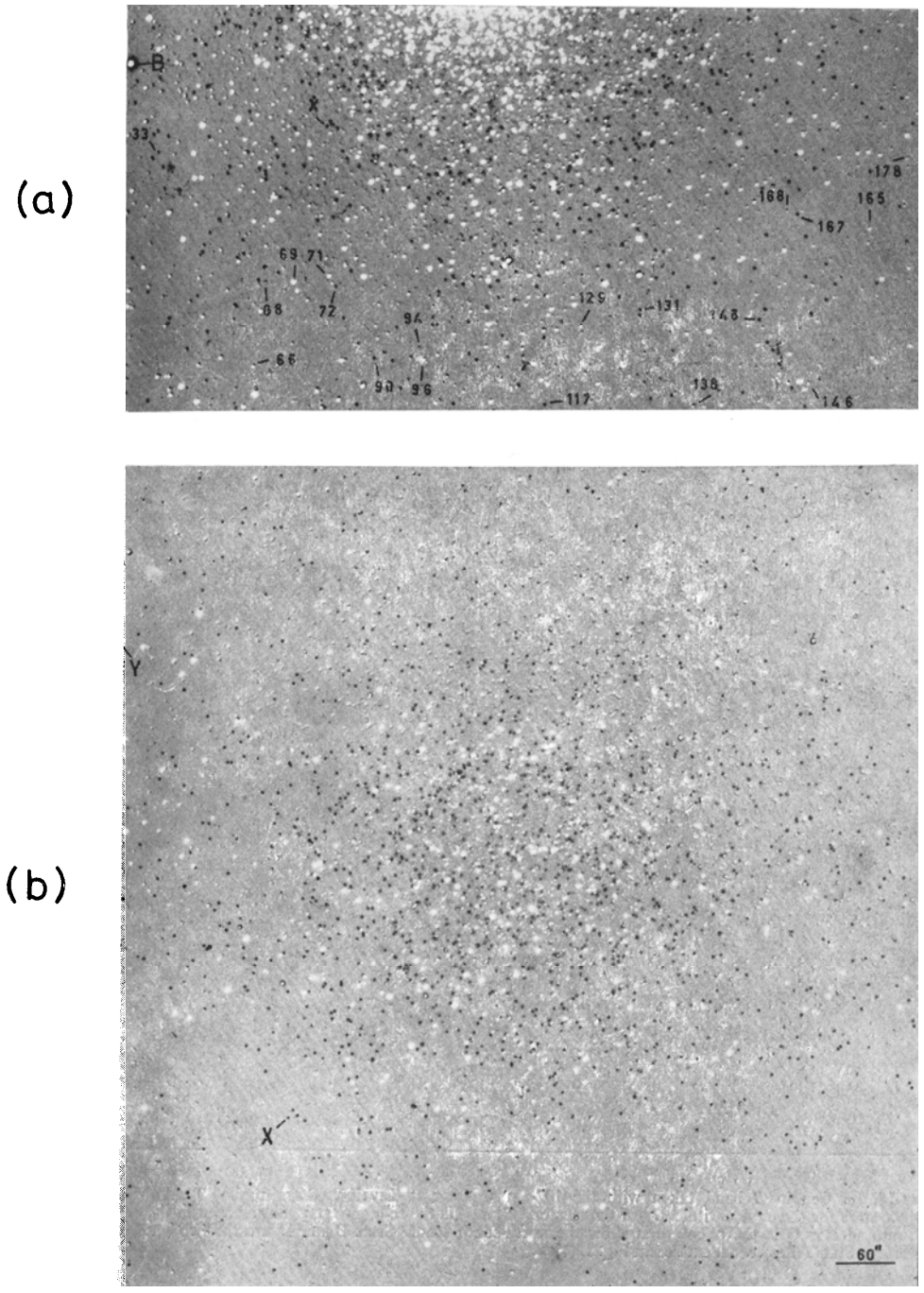

Figure 15. Distribution of Horizontal Branch stars in ω Cen. (a) Outer region: 20 stars with *UBV* photometry by Geyer (1967) are identified. Stars having colour $B - V < 0.4$ mag are seen as dark points while redder stars are seen as white points. (b) Inner region: Star X is marked to allow an easy comparison of the two figures.

change for a cluster with, such a small core radius; hence the exact location of the colour change cannot be determined from their observations.

In Section 2·3 we have pointed out the indirect evidence available for the presence of a bluer continuous background in the case of M 92 and M 3. Kadla *et al.* (1976) give the change in the ellipticity of these clusters from the inner to the outer regions. For M 92, the ellipticity increases from a = 100 arcsec to a maximum between 100 and 160 arcsec. This is also the region where the difference in the UV excess of AGB and GB stars is maximum as shown by Strom and Strom (1971). Hence we see that, even in this cluster, the background contribution has a relationship with the sudden increase in ellipticity of the cluster. Fig. 7 shows that the background effect is maximum within 2·8 arcmin from the centre of M 3. From Kadla *et al.* (1976) we find the ellipticity for M 3 increases from about 1·4 arcmin and reaches a maximum value around 2·7 arcmin. The red stars in the outer regions like those near the centre of the cluster, show a more spherical distribution as indicated by the decrease in the ellipticity of the cluster.

4. The Stars of the horizontal branch

In an earlier section we have shown the close association between the colour gradient across the cluster and the change in ellipticity with distance from the centre. We have also shown that a part of the contribution to the colour gradient is from a blue diffuse bulge of unresolved stars and that this bulge is characterised by a small UV excess. The main contribution to the colour gradient must be coming from the BHB stars. In this section, we describe the use of composite photography to separate out the blue and red stars in a globular cluster and study their distribution to explain the observed colour distribution over the cluster.

We know that ω Cen has a populated horizontal branch that is well separated in B — V colour, from the giant and the subgiant branch. All the HB stars have a colour B — V < 0·40 mag and the giant stars have B — V < 0·60 mag. Since it is a metal poor cluster, the asymptotic branch is not well populated and hence the blue stars are well separated from the red stars in the HR diagram. It is therefore easy to isolate them by photographic subtraction. In the case of horizontal branch stars, we have the added advantage that these stars are within a very small magnitude range and appear as stars with almost equal image diameters in the composite photograph. To avoid the main sequence, which is at best a minor contributor to the total brightness of the cluster, we have to control the exposure times of the original plates.

The blue plates are taken on 103a-O emulsion through a GG 11 filter. The infrared plates are on I-N emulsion through an RG 8 filter. Two kinds of composites are possible. In one case the negative of the blue plate is matched with the positive of the infrared plate (B^-I^+) and in the other case the negative of the infrared plate is matched with the positive of the blue plate (B^+I^-). Fig. 15 is a positive of a B^+I^- composite photograph of ω Cen. In such a picture, stars bluer than 0·40 mag are seen as black dots. Fig. 15(a) shows the blue stars in the outer regions of the cluster while in Fig. 15(b) we see the blue stars in the central regions of the cluster. Table 6 gives a list of stars taken from Geyer (1967) for which *UBV* magnitudes have been determined. These have been marked in Fig. 15(a). Star X is marked in both the pictures to allow an easy comparison. It is very clear that all stars bluer than 0·40

Table 6. Geyer numbers of stars identified in Fig. 15(a).

Geyer Number	V	$B-V$	$U-B$
B	8·78	−0·01	−0·12
33	15·34	−0·04	−0·31
66	13·90	1·01	0·10
68	14·95	−0·03	0·05
69	12·26	1·29	0·83
71	12·92	1·23	0·20
72	15·01	0·05	−0·17
90	15·07	−0·08	−0·12
94	15·06	−0·19	−0·03
96	13·48	0·94	0·08
117	14·97	−0·05	0·03
129	14·04	1·03	0·01
131	14·57	0·15	0·02
138	13·52	0·49	−0·05
146	13·05	0·56	0·06
148	14·75	−0·08	0·18
165	13·39	0·98	0·37
167	14·78	0·03	0·02
168	14·66	0·83	−0·06
178	15·02	0·60	−0·11

mag appear as black dots in the picture. We have counted these blue stars with the aid of a grid of the kind shown in Fig. 16. The total counts per unit area in each annular ring of width 34 arcsec provides an idea of the density distribution. The values marked outside the outermost ring in Fig. 16 are the total counts in each sector. These values show the cluster ellipticity very well. The position angle of the major axis is about 70° which is much smaller than the value obtained for the cluster in V band equidensitometry. Thus the position angle is about 110° for the cluster core, about 100° for the region between 2 arcmin and 6 arcmin and about 70° for the system of blue stars.

In Fig. 17(a) we have compared the distribution of the HB stars in ω Cen with its surface brightness in the I and U bands. Fig. 17 (b) shows log N_{HB} against r_e where N_{HB} is the number of HB stars per arcmin^2 and r_e is the effective distance of the annular zone given by $r_e = \{[\frac{1}{2}\ (r_1^2 + r_2^2)]\}^{1/2}$, r_1 and r_2 being the inner and the outer radii of the annulus. The data for Fig. 17(a) are taken from Table 3. Since the contribution from the blue stars to the I band is negligible, we may assume that the I band surface brightness is indicative of the distribution of the GB stars in the cluster. From Fig. 17(a), the GB stars can be seen decreasing in density from the centre. The number density of the HB stars exhibits a general drop with distance from the centre; the striking feature is an enhancement over the normal gradient between 1·5 arcmin and 4·5 arcmin. It is this relative increase in the number of HB stars over the bright red giants in the 2 arcmin to 4 arcmin zone that gives much of the blue colour to the cluster seen in Fig. 5 between 1·5 arcmin and 4·5 arcmin. The system of HB stars shows a more elliptical distribution when compared to the system of red stars and also has a different position angle for the major axis. Thus all the; available, evidence shows the presence of a blue bulge of resolved and

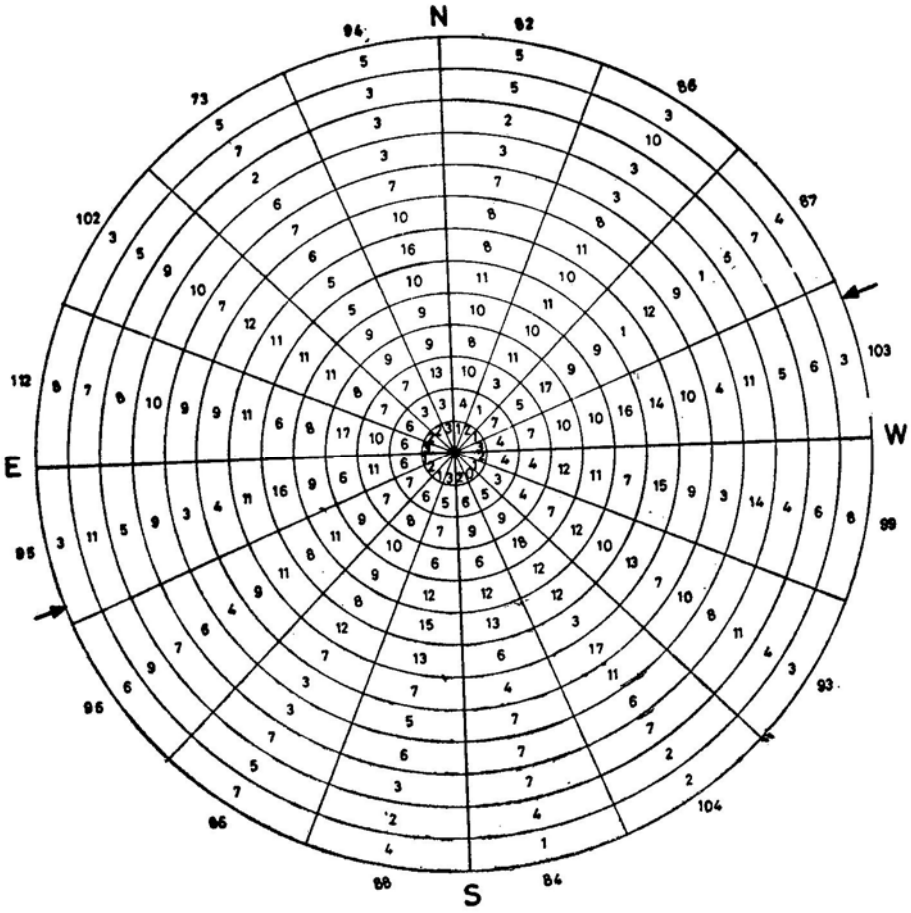

Figure 16. Counts of the horizontal branch stars in the inner regions of the cluster ω Cen. The grid shown in the figure is the kind used for counting the stars. The east-west line is marked on the grid, the centre of which is exactly superposed on the centre of the cluster determined from equi-densitometry. The numbers marked outside the outermost ring are the total counts for each sector. Also marked in the figure (arrows) is the position angle of the inner region of the cluster.

unresolved stars with a distribution different from that of the giant stars in the cluster.

The horizontal branch stars show a larger number density in the region between 1·7 arcmin and 4 arcmin in ω Cen. This cluster is well known for its wide giant branch which is indicative of a large range in metal abundance in the GB Stars. Norris (1980) has reported that the H and K lines of singly ionised Calcium and also the CN features vary greatly in strength from one giant to another in ω Cen. The colour-abundance corelation is so well established for the giants that the colour of a giant at a given magnitude is taken as a measure of its abundance. Freeman and Rodgers (1975) find that there is a large spread in the [Ca/H] values for the 25 RR Lyrae stars they observed. This indicates a primordial abundance variation in the gaseous cloud which formed ω Cen. Globular clusters are very old stellar systems and hence we should expect mass segregation in them. Theoretical considerations show that a metal rich main sequence star takes much longer to reach the giant stage than a metal

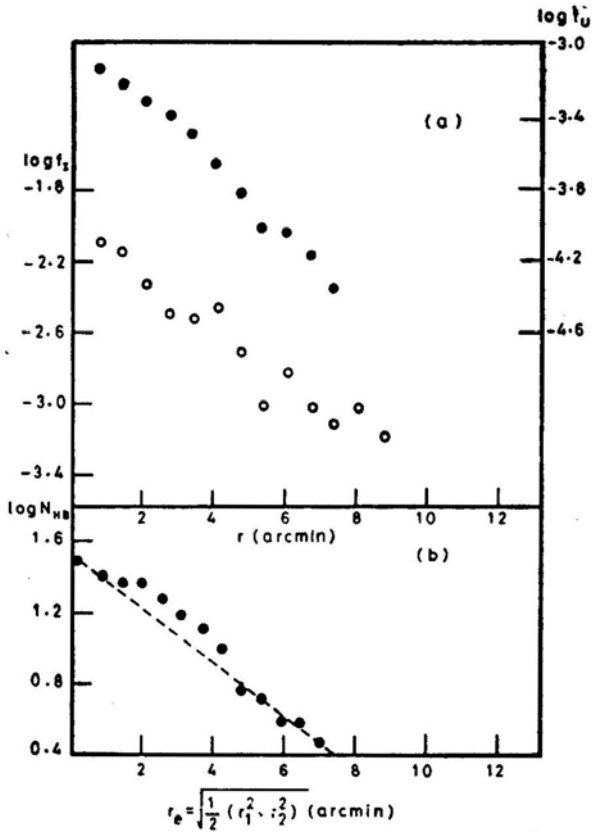

Figure 17. (a) The surface brightness profiles for ω Cen in U and the infrared bands. The filled circles represent log f values in U (scale at right) while the open circles denote the infrared values (scale at left). (b) The variation of the number of HB stars (N_{HB}) per arcmin^2 as a function of distance from the centre.

poor star. If two stars-one metal poor and the other metal rich-reach the giant stage at the same time, then the metal rich star should have started with a larger mass, so that the increase in the evolution time from the main sequence to the giant branch is compensated by the decrease in it due to a larger initial mass. Hence, at any time, a metal poor giant branch star is less massive than a metal rich giant branch star. For stars of mass close to that of the Sun and lower, the evolution time from the main sequence to the giant stage is much longer than the relaxation time at the centre of the cluster. Hence the metal poor giants can have a larger spatial distribution in be confined to the core. Thus, in ω Cen, giant stars which are metal poor compared to the red giants forming the core of the cluster, should find themselves at larger distances from the centre. These stars, when they evolve to the HB stage will continue to have the same distribution, since the evolution time from GB to HB is much shorter than the relaxation time of the cluster. This can explain the presence of a larger BHB to GB ratio and the resultant bluer colour for the intermediate region in ω Cen. It is difficult to speculate on the nature of the diffuse background Similar to the HB stars, the stars forming the background also have a small UV

excess. The contribution of white dwarfs to this background would also be very significant.

5. Nucleus of M 31 and ω Centauri

Using Stratoscope pictures of M 31, Light, Danielson and Schwarzschild (1974) have shown that the nucleus of M 31 is a separate and distinct feature of the Galaxy. It is found to be elliptical (1 arcsec × 1·6 arcsec) with its major axis lying in a position angle of 63° ± 5°. The position angle of M 31 is 38° (Johnson 1961). Light, Danielson and Schwarzschild find a sharp discontinuity of the nucleus from the nuclear bulge. They suggest that, as the nucleus and bulge are separate features, they would exhibit different velocity dispersions, colour, metallicity *etc.* which can be detected from ground based observations.

Walker's (1974) rotation curve of the nucleus of M 31 peaks with V_r= 100 km s^{-1} at r = 2·2 arcsec. The rotation curve falls in a Keplerian manner beyond r = 2·2 arcsec. Peterson (1978) has measured the rotation in the nuclear region of M 31 and obtained a peak velocity of V_r= 60 km s^{-1} at r = 1·5 arcsec. He finds that the velocity drops to zero between 3 arcsec and 6 arcsec before increasing once again. This rotation curve is explained using a two-component dynamical model, one component representing the nucleus and the other representing the nuclear bulge. The bulge component which dominates the surface brightness beyond 2 arcsec ($\simeq$ 6·5 pc) has a major axis luminosity profile with a core radius of 20 arcsec (from a fit of King's model).

In the case of ω Cen we have seen that the values of core radii are larger at shorter wavelengths than in the near infrared. We have also pointed out the correspondence between the locations of a blue bulge and the change in ellipticity of the isophotes. This bulge seems to contain a large number of AGB and HB stars as derived from their δ (U — B) characteristic. If we assume that a larger ellipticity is the result of a higher velocity of rotation, then the bulge in ω Cen should be rotating faster than the core. In the results obtained by Walker, the region of maximum rotational velocity falls well outside the nucleus. The core size of ω Cen in the light of the B band is about 2·5 pc in radius, whereas for the nucleus of M 31 the value is $\simeq$ 5 pc. The maximum ellipticity in ω Cen is at 6 pc and the maximum rotational velocity in the nucleus of M 31 is at 7·5 pc (Walker 1974). Peterson (1978) shows a dip in the velocity of nuclear rotation in M 31 between 10 pc and 20 pc from the centre. For ω Cen also we see a decrease in ellipticity between 6 pc and 8 pc. Beyond this region the ellipticity in the globular cluster and the rotation in the nucleus of M 31 show a gradual increase.

The similarity between the nucleus of M 31 and ω Cen in the photometric aspects of behaviour seems real and not fortutious. Dynamical causes, as yet unknown, may be responsible for the existence of sub-systems with characteristics that are subtly revealed by some aspects of integrated photometry. As we are on the threshold of high resolution studies of such galactic nuclei, the similarities seen over a range of stellar aggregates with a range of masses would undoubtedly contribute greatly to their elucidation.

References

Arp, H. C. 1958, *Astr. J.*, **63**, 118.
Cathey, L. R. 1974, *Astr. J.*, **79**, 1370.
Chun, M. S., Freeman, K. C. 1979, *Astrophys. J.*, **227**, 93.
Da Costa, G. S. 1979, *Astr. J.*, **84** , 505.
Dickens, R. J., Woolley, R. v.d. R. 1967, *R. Obs. Bull*, No. 128.
Eggen, O. J., Sandage, A. R. 1965, *Astrophys. J.*, **141**, 821.
Fernie, J. D. 1974, *Publ. astr. Soc. Pacific*, **86**, 837.
Freeman, K. C., Rodgers, A. W. 1975, *Astrophys. J.*, **201**, L71.
Gascoigne, S C. B., Burr, E. J. 1956, *Mon. Not. R. astr. Soc.*, **116**, 570.
Geyer, E. H. 1967, *Z. Astrophys.*, **66**, 16.
Hartwick, F. D. A. 1970, *Astrophys. J.*, **161**, 845.
Högner, W., Kadla, Z. I., Richter, N., Strugatskaya, A. A. 1973, *Soviet Astr.*, **16,** 843.
Illingworth, G., Illingworth, W. 1976, *Astrophys. J. Suppl. Ser.*, **30,** 227.
Iriarte, B., Johnson, H. L., Mitchell, R. I., Wisnieswski, W. 1965, *Sky Telesc.*, **30,** 21.
Johnson, H. L., Sandage, A. R. 1956, *Astrophys. J.*, **124,** 379.
Johnson, H. M. 1961, *Astrophys. J.*, **133,** 309.
Kadla, Z. I. 1966, *Soviet Astr.* **10,** 97.
Kadla, Z. I., Richter, N., Strugatskaya, A. A., Högner, W. 1976, *Soviet Astr.*, **20,** 49.
King, I. R. 1962, *Astr. J.*, **67,** 471.
King, I. R. 1966a, *Astr. J.*, **71,** 64.
King, I. R. 1966b, *Astr. J.*, **71,** 276.
Light, E. S., Danielson, R. E., Schwarzschild, M. 1974, *Astrophys. J.*, 1**94,** 257.
Lindsay, Ẽ. M. 1956, *in Vistas in Astronomy*, Ed. A. Beer, Pergamon Press, New York, p. 1057.
Martin, W. Chr. 1938, *Ann. Sterrew. Leiden*, XVII, Part 2.
Norris, J. E. 1980, in *Globular Clusters*, Ed. D. Hanes and B. Medore, Cambridge University Press, P. 113.
Norris, J., Bessell, M. S. 1975, *Astrophys. J.*, **201,** L76.
Oort, J. H., van Herk, G. 1959, *Bull. astr. Inst. Netherl.* **14,** 299.
Peterson, C. J. 1978, *Astrophys. J.*, **221,** 80.
Peterson, C. J., King, I. R. 1975, *Astr. J.*, **80,** 427.
Poveda, A., Allen, C. 1975, *Astrophys. J.*, **197,** 155.
Rusev R. M. 1974, *Sov. Astron.*, **18,** 71.
Sandage, A. R. 1953, *Astr. J.*, **58,** 61.
Sandage, A. 1957, *Astrophys. J.*, **125,** 422.
Sandage, A. 1970, *Astrophys. J.*, **162,** 841.
Sandage, A., Walker, M. F. 1966, *Astrophys. J.*, **143,** 313.
Scaria, K. K. 1980, *Kodaikanal Obs. Bull*, (in press).
Sistero, R. F., Fourcade, C. R. 1970, *Astr. J.*, **75,** p. 34.
Strauss, F. M. 1978, *Astr. Astrophys. Suppl. Ser.*, **33,** 315.
Strom, S. E., Strom, K. M. 1971, *Astr. Astrophys.*, **14,** 111.
Strom, S. E., Strom, K. M., Goad, J. W. 1976, *Astrophys. J.*, **204,** 684.
Walker, M. F. 1974, *Publ. astr. Soc. Pacific*, **86,** 861.